Impact of the Ocean's Overturning Circulation on Atmospheric CO_2

Andreas Schmittner

College of Oceanic and Atmospheric Sciences, Oregon State University, Corvallis, Oregon, USA.

Edward J. Brook and Jinho Ahn

Department of Geosciences, Oregon State University, Corvallis, Oregon, USA.

A coupled climate-carbon cycle model and ice core CO_2 data from the last glacial period are used to explore the impact of changes in ocean circulation on atmospheric CO_2 concentrations on millennial time scales. In the model, stronger wind driven circulation increases atmospheric CO_2. Changes in the buoyancy driven deep overturning in the Atlantic affect atmospheric CO_2 only indirectly through their effect on Southern Ocean stratification. In simulations with an abrupt and complete shutdown of the Atlantic overturning, stratification in the Southern Ocean decreases due to salinification of surface waters and freshening of the deep sea. Deeper mixed layers and steeper isopycnals lead to outgassing of CO_2 in the Southern Ocean and hence gradually increasing atmospheric CO_2 concentrations on a multi-millennial time scale. The rise in CO_2 terminates at the time of rapid resumption of deep water formation and warming in the North Atlantic, and CO_2 levels subsequently gradually decrease. These model responses and a strong correlation between simulated atmospheric CO_2 and Antarctic surface air temperatures with little or no time lag are consistent with newly synchronized ice core data from the last ice age. Sensitivity experiments reveal that the amplitude of the response of atmospheric CO_2 is sensitive to the model background climatic state and decreases in a colder climate owing to smaller changes in the overturning.

INTRODUCTION

The ocean contains 60 times as much carbon as the atmosphere and 17 times as much as the terrestrial biosphere including soils [*Sarmiento and Gruber*, 2006]. As such it is thought to exert a strong control on the concentration of CO_2 in the atmosphere, and hence on climate, on time scales of centuries to thousands of years. The ocean affects atmospheric CO_2 through physical and biological processes. Carbon-rich cold water (due to greater solubility at lower temperatures) sinks at high latitudes and fills the deep ocean, leading to larger carbon concentrations at depths. This "solubility pump" accounts for 30-40% of the surface to deep gradient of dissolved inorganic carbon (DIC) (*Toggweiler et al*., 2003; see also below e.g. lower left panel in Figure 2). Biological activity removes carbon from the surface along with nutrients in the form of sinking particulate organic matter (POM) and calcium carbonate ($CaCO_3$) shells which is remineralized back to inorganic matter or dissolves in the abyss. This "biological pump" accounts for 60-70% of the surface to deep DIC gradient. Sinking of $CaCO_3$ leads to a vertical gradient in alkalinity. Its production, though changes in the carbonate ion chemistry, increases the partial pressure P_{CO2} of CO_2 in surface waters and hence atmospheric CO_2. Both the solubility as well as the biological pump are affected by the ocean's circulation.

Ocean Circulation: Mechanisms and Impacts
Geophysical Monograph Series 173

10.1029/173GM20

Models

How exactly do changes in ocean circulation affect atmospheric CO_2 concentrations? A number of previous modeling studies have addressed this question with different and sometimes conflicting results. *Siegenthaler and Wenk* [1984] find a decrease of CO_2 if the deep overturning circulation is increased in their 4 box ocean-atmosphere model. In the similar model of *Sarmiento and Toggweiler* [1984] the response of atmospheric CO_2 to changes in the deep overturning circulation depends qualitatively on the exchange between the surface and deep ocean at high latitudes. If this exchange is high or intermediate, increased circulation leads to lower CO_2; if it is low, CO_2 increases. Both models assume invariant and near zero surface nutrient concentrations at low latitudes but variable concentrations at high latitudes. Both models are sensitive to high latitude processes and predict an increase of CO_2 if vertical mixing in the Antarctic ocean is larger. In an idealized, albeit 3 dimensional, ocean model setup, *Toggweiler et al*. [2006] recently demonstrated that large self sustained atmospheric CO_2 oscillations of 30-45 ppmv can result from fluctuations in Southern Ocean stratification induced by changes in the wind stress.

Marchal et al. [1998, 1999], using a zonally averaged ocean model, found that CO_2 increased in transient simulations after North Atlantic Deep Water (NADW) formation was shut down by freshwater input to the North Atlantic. They suggested decreased solubility of CO_2 in warmer surface waters in the Southern Ocean as the main explanation for higher atmospheric CO_2. Contrary to those results other models predict an increase of CO_2 with stronger NADW formation [*Keir*, 1988; *Heinze and Hasselmann*, 1993; *Schulz et al*., 2001; *Köhler et al*., 2005a, 2006].

Studies with stand alone terrestrial vegetation models [*Scholze et al*., 2003; *Köhler et al*., 2005b] find higher atmospheric CO_2 due to reduced carbon storage on land brought about by climate changes associated with a reduction of the deep Atlantic overturning circulation.

Observations

Observations of CO_2 variations obtained by measuring air trapped in bubbles of ancient ice from Antarctica [*Indermühle et al*., 2000], provide a unique opportunity to test carbon cycle models on multi-millennial time scales. Figure 1 shows a new synchronization of these CO_2 measurements based on CH_4 correlation between Greenland and Taylor Dome, Antarctica [*Ahn and Brook*, 2007]. Due to the low resolution of the Taylor Dome CH_4 record the age model takes also into account newly measured high-precision Byrd CO_2 records between 47 and 65 ka [*Ahn and Brook*, 2007] and previously published CO_2 records from the Byrd ice core from 30 to 46 ka [*Neftel et al*., 1988].

The following important features are apparent in these observations and robust with respect to dating uncertainties: (1) gradually increasing CO_2 concentrations during some (but not all) cold times (stadials) in Greenland. Throughout this paper we also assume that stadials are associated with reduced deep overturning in the North Atlantic, adopting previous hypotheses [*Broecker et al*., 1985] and numerous data (see e.g. the review paper by *Broecker* in this volume) and model studies [e.g. *Schmittner et al*., 2002, 2003] although this view is not uncontested (see article by *Wunsch* in this volume). The Greenland stadials associated with CO_2 increase also correspond to events of widespread ice rafting in the North Atlantic (Heinrich events 4, 5, 5a, and 6). (2) CO_2 concentrations peak at the same time (within the dating uncertainty) of large rapid warming events in Greenland that signal an abrupt resumption of a vigorous overturning circulation. (3) After this transition CO_2 gradually decreases during prolonged warm (interstadial) episodes in Greenland. (4) A strong correlation exists between surface air temperatures over Antarctica and atmospheric CO_2. (5) Antarctic temperatures and atmospheric CO_2 vary on a multi-millennial time scale and do not show the abrupt transitions and higher frequency variations present in the Greenland temperature and methane records. Longer stadials in Greenland are associated with larger amplitude warming events in Antarctica (*EPICA Community Members*, 2006). Any successful theory or model simulation needs to reproduce the five features listed above.

In summary, ice core data suggest a correlation between ocean circulation and atmospheric CO_2 on millennial time scales whereas results from previous modeling appear conflicting and inconsistent and there is no generally accepted theory as to whether atmospheric CO_2 should increase or decrease due to a stronger ocean circulation. In addition, all previous model studies were carried out with highly simplified models (either box models, or zonally averaged ocean circulation models) that did not incorporate important physical (such as three dimensional deep and intermediate water circulation in the Southern Ocean or dynamical sea ice) or biological (such as the explicit representation of phytoplankton) processes. Here we try to illuminate the effect of both changes in the ocean's wind and buoyancy driven overturning circulations on atmospheric CO_2 using a detailed 3-dimensional model of ocean circulation, ecosystem dynamics and carbon cycling embedded in a coupled climate model of intermediate complexity including an interactive dynamic terrestrial vegetation component.

A WORKING HYPOTHESIS

Let us, as a working hypothesis, assume that increasing the ocean circulation leads to higher atmospheric CO_2. This hypothesis can be rationalized by the following thought experiment. Consider that biological activity always removes nutri-

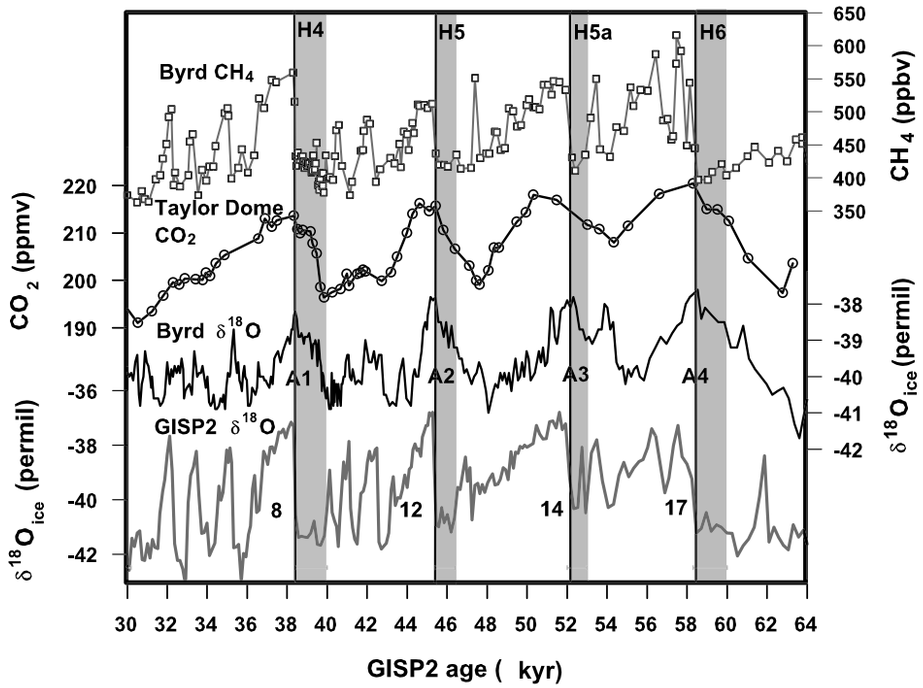

Figure 1. Comparison of atmospheric CO_2 and climate changes during the last ice age from *Ahn and Brook* (2007). Open square, CH_4 from Byrd ice core, Antarctica [*Blunier and Brook*, 2001]; open circle, CO_2 from Taylor Dome, Antarctica [*Indermühle et al*., 2000]; black line, $\delta^{18}O_{ice}$, as a proxy of surface temperature, from Byrd station, Antarctica [*Johnsen et al*., 1972] on the timescale of *Blunier and Brook* [2001]; gray line, $\delta^{18}O_{ice}$ from Greenland Ice Sheet Project 2 (GISP2) ice core (Summit, Greenland) [*Grootes et al*., 1993]. CO_2 from Taylor Dome is synchronized with GISP2 age [*Ahn and Brook*, 2007] using CH_4 from Taylor Dome [*Brook et al*., 2000] and CO_2 from Byrd station [*Ahn and Brook*, 2007; *Neftel et al*., 1988]. Vertical lines denote the peak of Antarctic warm events A1-A4 which are associated with rapid transitions from a cold stadial to warm interstadial state in Greenland. Gray shaded bars represent Heinrich events [*Sarnthein et al*., 2001; *Rashid et al*., 2003]. Dansgaard/Oeschger warm events 8, 12, 14 and 17 and Heinrich events 4, 5, 5a and 6 are denoted by numbers. Note that following these stadial to interstadial transitions atmospheric CO_2 decreases gradually on a multi-millennial time scale.

ents and carbon from the ocean surface due to the sinking of particulate organic matter. Plankton productivity is maintained only because the ocean circulation returns remineralized inorganic nutrients and carbon to the sunlit surface. Thus, in the limit of a motionless ocean, surface waters would be stripped of all nutrients, and DIC concentrations (and hence atmospheric CO_2) would be low. In the limit of an infinitely strong circulation the deep and surface waters would be well mixed and surface nutrients, and DIC, and atmospheric CO_2 would be high. In other words: in this case the biological and solubility pumps would not be able to establish any vertical DIC gradient.

The atmospheric CO_2 concentration in such a world of a well mixed ocean can easily be calculated as the partial pressure of CO_2 (P_{CO2}) in equilibrium with sea water with its preindustrial global mean temperature (4°C), salinity (34.9), DIC (2.304 mmol/m^3) and alkalinity (2.417 mmol/m^3) concentrations as 518 ppmv (1 ppmv P_{CO2} = 2.13 gigatons of carbon [GtC]). This is almost twice the preindustrial atmospheric CO_2 concentration of 280 ppmv and presents an upper limit of the effect of ocean circulation on atmospheric CO_2. This value is consistent with model experiments in which the solubility and biological pumps were switched off [*Cameron et al*., 2005]. Our hypothesis assumes finite plankton growth rates as well as a constant terrestrial carbon pool. The term "ocean circulation" refers to any vertical water exchange, either by convection, eddy activity, or the large scale overturning circulation. Thus, our hypothesis suggests a simple relationship between ocean circulation and atmospheric CO_2, such that a stronger circulation leads to higher CO_2.

Below we will present model experiments designed to test this hypothesis and to quantify the effect of changes in ocean circulation on atmospheric CO_2 concentrations. After a description of the model in the following section, we present experiments in which the wind driven circulation and the buoyancy driven circulation (both through changes in surface fluxes and interior mixing) have been changed and the response of the global coupled carbon cycle has been analyzed in order to understand the simulated changes in atmospheric CO_2.

MODEL DESCRIPTION AND ANALYSIS

The physical model is based on the University of Victoria Earth System Climate Model [*Weaver et al*., 2001] version 2.7. It includes a global, three dimensional, primitive equations, ocean model with diffusion along and across isopycnal surfaces, a parameterisation of tracer advection due to eddies [*Gent and McWilliams*, 1990] and a tidal mixing scheme [*Simmons et al*., 2004]. This scheme leads to enhanced vertical mixing over rough topography and results in low diapycnal mixing in the pelagic pycnocline with diapycnal diffusivities K_v there equal to the background diffusivity $K_b = 2 \times 10^{-5} m^2 s^{-1}$. A simple, two dimensional energy balance model of the atmosphere is used with a prescribed seasonal cycle of winds as well as an interactive dynamical terrestrial vegetation/carbon cycle model [*Meissner et al*., 2003]. Of particular importance in this study is a state of the art dynamic-thermodynamic sea ice model which strongly improves stratification and deep and intermediate water formation in the Southern Ocean [*Saenko et al*., 2002].

The marine ecosystem model is an improved version of *Schmittner et al*. [2005] with a parameterization of fast nutrient recycling due to microbial activity after *Schartau and Oschlies* [2003]. It considers two phytoplankton classes (nitrogen fixers and other phytoplankton), one zooplankton class, sinking particulate organic matter (detritus) as well as interactive cycling of nitrogen, phosphorus and oxygen including denitrification in low oxygen waters [*Schmittner et al*., in press]. The inorganic variables include oxygen (O_2), two nutrients, nitrate (NO_3) and phosphate (PO_4) as well as DIC and total alkalinity (ALK). They are linked through exchanges with the biological compartments via Redfield stoichiometry ($R_{P:N} = 1/16$, $R_{O:N} = 13$, $R_{C:N} = 7$).

Calcium carbonate ($CaCO_3$) production is parameterized as a fixed ratio ($r_{CaCO3:C} = 0.028$) of the net production of POM in the water column. Because of nutrient and carbon recycling within the euphotic zone (regeneration), net production of POM is always larger than export production of POM out of the euphotic zone. We assume that $CaCO_3$ is not recycled within the euphotic zone but immediately exported because $CaCO_3$ sinks much faster than POM. The parameter $r_{CaCO3:C}$ has been tuned to reproduce the global vertical ALK gradient. Thus the rain ratio of calcite to organic matter flux at the base of the euphotic zone (~100m) is variable in our model and depends e.g. on nutrient cycling within the euphotic zone. As shown in *Schmittner et al*. (submitted manuscript) its values and latitudinal distribution (are consistent with recent observational estimates [*Sarmiento et al*., 2002]. Dissolution of $CaCO_3$ is determined by instantaneous sinking with an e-folding depth of 3500m.

Formulations of air-sea gas exchange and carbon chemistry follow protocols from the Ocean Carbon-Cycle Model Intercomparison Project [OCMIP, *Orr et al*., 1999] as described in *Ewen et al*. [2004]. One deviation from the OCMIP protocol is the treatment of the effect of freshwater fluxes on surface DIC and ALK. Here we follow the approach of *Marchal et al*. [1998] and use a salinity normalized tracer, e.g.: $DIC_m = DIC \cdot \overline{S} / S$, where DIC_m is the model value without dilution/concentration by surface freshwater fluxes and DIC the actual in situ value, S is the local salinity and $\overline{S} = 34.9$ is a reference salinity. In the calculation of air-sea gas exchange and surface chemistry as well as for comparison with observations DIC is used. This method avoids the use of virtual freshwater fluxes at the surface but sensitivity tests showed that resulting surface P_{CO2} and air-sea fluxes are very similar for both methods.

A more complete description of the model as well as a detailed comparison with present day observations will be given elsewhere (*Schmittner et al*., submitted manuscript.). There it is also shown that the model is consistent with a large array of observations including radiocarbon (bomb and natural), anthropogenic carbon and chlorofluorocarbons, as well as air-sea fluxes of CO_2. For example, the model versions used here are consistent with all metrics proposed by *Matsumoto et al*. [2004].

Here, we use two model versions termed wNPs and sNPs in Tables 1 and 2. Model version wNPs exhibits a *w*eak *N*orth *P*acific *s*tratification caused by an underestimated halocline. In order to correct this systematic bias model version sNPs (*s*trong *N*orth *P*acific *s*tratification) was constructed by adding 0.1 Sv of freshwater permanently to the North Pacific north of 40°N (a compensating flux in the rest of the world ocean was used in order to conserve global salinity). This flux correction has the desired effect of increasing the stratification and improves tracer distributions such as oxygen and nutrients in the North Pacific (not shown); however, it is not clear whether or not such a permanent flux correction biases the transient model response. The use of both model versions circumvents this problem. It is also motivated by the fact that the response of the North Pacific circulation to a perturbation of the Atlantic overturning depends on the stratification there [*Schmittner and Clement*, 2002]. During the glacial, stratification in the North Pacific was most likely different from today. Stable isotope records from below 1 km depth suggest better ventilation of the upper ocean [*Keigwin*, 1998], whereas it was inferred from surface productivity records that stratification in the glacial North Pacific was larger than today [*Jaccard et al*., 2005]. Here we use both model versions in order to test the robustness and sensitivity of our results to different stratification in the North Pacific.

Atmospheric CO_2 is calculated fully prognostically in one well-mixed atmospheric box and its changes interactively

affect the radiative balance and hence climate. Due to remaining model imperfections the simulated preindustrial atmospheric CO_2 concentration is 308 ppmv, slightly higher in both model versions than the observed value of ~280 ppmv. The simulated oceanic carbon inventories, however, as well as the 3-dimensional patterns of dissolved inorganic carbon and alkalinity distributions are consistent with observational estimates as will be shown below.

In order to separate the contributions of the biological and solubility pump we use a model version with an abiotic ocean carbon cycle only (termed NoBio in the following). In this model version surface alkalinity is fixed at its observed global mean value of $2.36775 \cdot S / \overline{S}$ mol/m^3. The lower left panel in Figure 2 shows that in our model the solubility pump accounts for only 1/3 of the surface to deep DIC gradient, whereas the biological pump accounts for 2/3.

To our knowledge this is the most complete and detailed model yet applied to study the impact of ocean circulation changes on atmospheric CO_2 on millennial time scales. However, it needs to be clearly stated that certain processes are still highly simplified. Atmospheric heat and moisture transports, for instance, are not influenced by changes in wind velocities. Wind stress to the ocean and sea ice is prescribed as well and does not respond to climatic changes. We will address some of these model simplifications and their possible influences on reported results and conclusions below and in the discussion section. Most of our simulations have been performed for a preindustrial background climate. However, we do include one idealized experiment using a colder, more glacial background climate in a sensitivity test.

Analysis of Ocean Circulation and P_{CO2} Changes

Table 1 presents indices of the large scale circulation in different model simulations close to equilibrium, whereas Table 2 lists important variables of the carbon cycle in those simulations. The atmospheric concentration of CO_2 is strongly controlled by the sea surface P_{CO2}. This can be seen in similar (albeit not exactly the same) changes of atmospheric CO_2 and surface ocean P_{CO2} in the different experiments listed in Table 2. Differences between atmospheric CO_2 and sea surface P_{CO2} are caused by changes in air-sea equilibration, e.g. due to changes in sea ice cover or changes in the residence time of surface waters. In the model, sea surface P_{CO2} depends only on temperature T, salinity S, DIC and ALK: $P_{CO2} = P_{CO2}$(T,S,DIC,ALK), however non-linearly. This allows decomposition of the simulated total changes of P_{CO2} into individual contributions [*Marchal et al*., 1998]. In Table 2 we show P_{CO2} changes brought about by variations of T and S that determine primarily physical solubility of surface waters ΔP_{CO2}(T,S) separately from changes brought about by redistributions of DIC and ALK which involve changes in biological and physical cycling ΔP_{CO2}(D,A). For example, the solubility effect is calculated as ΔP_{CO2}(T,S) = P_{CO2}(T(EXP),S(EXP), DIC(CTR),ALK(CTR)) − P_{CO2}(T(CTR),S(CTR),DIC(CTR), ALK(CTR)), where EXP denotes the equilibrium at the end of the experiment and CTR denotes the end of the corresponding control run. Generally, P_{CO2} changes caused by changes in S are small, thus the variations in P_{CO2}(T,S) reported in Table 2 are mainly caused by changes in T. Changes due to DIC are generally of opposite sign as those due to ALK [*Marchal et al*., 1998]. Note that due to non-linearities in the P_{CO2} equation, the sum of the changes due to T and S, and the changes due to DIC and ALK does not need to add up exactly to the total P_{CO2} change.

WIND DRIVEN CIRCULATION

In this section two idealized experiments are discussed, in which the wind stress everywhere at the surface of the ocean and sea ice was halved (0.5 × WS) or doubled (2 × WS). The shallow wind driven overturning circulation responds approximately linearly to these changes in the forcing. In the control run tropical Ekman cells in the northern (40 Sv) and southern (54 Sv) hemisphere amount to equatorial upwelling of 94 Sv. In the Pacific between 9°N and 9°S 42 Sv upwell across 50m into the model surface layer consistent with observational estimates of 41 ± 6 Sv [*McPhaden and Zhang*, 2002]. In experiment 0.5 × WS the tropical overturning cells are reduc ed to 22 Sv and 28 Sv, respectively, and in experiment 2 × WS equatorial upwelling is increased to 193 (= 90 + 103) Sv. The Antarctic Circumpolar Current (ACC) accelerates from 80 Sv in the control run "wNPs ctr" to 147 Sv in 2 × WS and decelerates to 54 Sv in 0.5 × WS. The Indonesian Throughflow, with 19 Sv in the control run consistent with observational estimates of 16 ± 5 Sv [*Ganachaud and Wunsch*, 2000], slows to 13 Sv in 0.5 × WS and speeds up to 27 Sv in 2 × WS.

Increasing the wind stress leads not only to a more vigorous upper ocean circulation but it increases deep overturning as well (Table 1). Upwelling in the Southern Ocean increases as does the rate of formation and export of NADW. These results are consistent with earlier findings [*Toggweiler and Samuels*, 1995] suggesting increased wind stress over the Southern Ocean leads to more Ekman suction of water from the deep ocean and thus to intensified NADW formation. In our case, additionally to this effect a more vigorous low latitude Ekman circulation increases subduction of warm surface water into the thermocline and leads to a deepening of the pycnocline at low latitudes which intensifies the meridional pressure gradients and thus accelerates the buoyancy driven deep overturning as well.

This acceleration of the surface and deep flows leads to faster nutrient delivery to the surface and thus has a strong

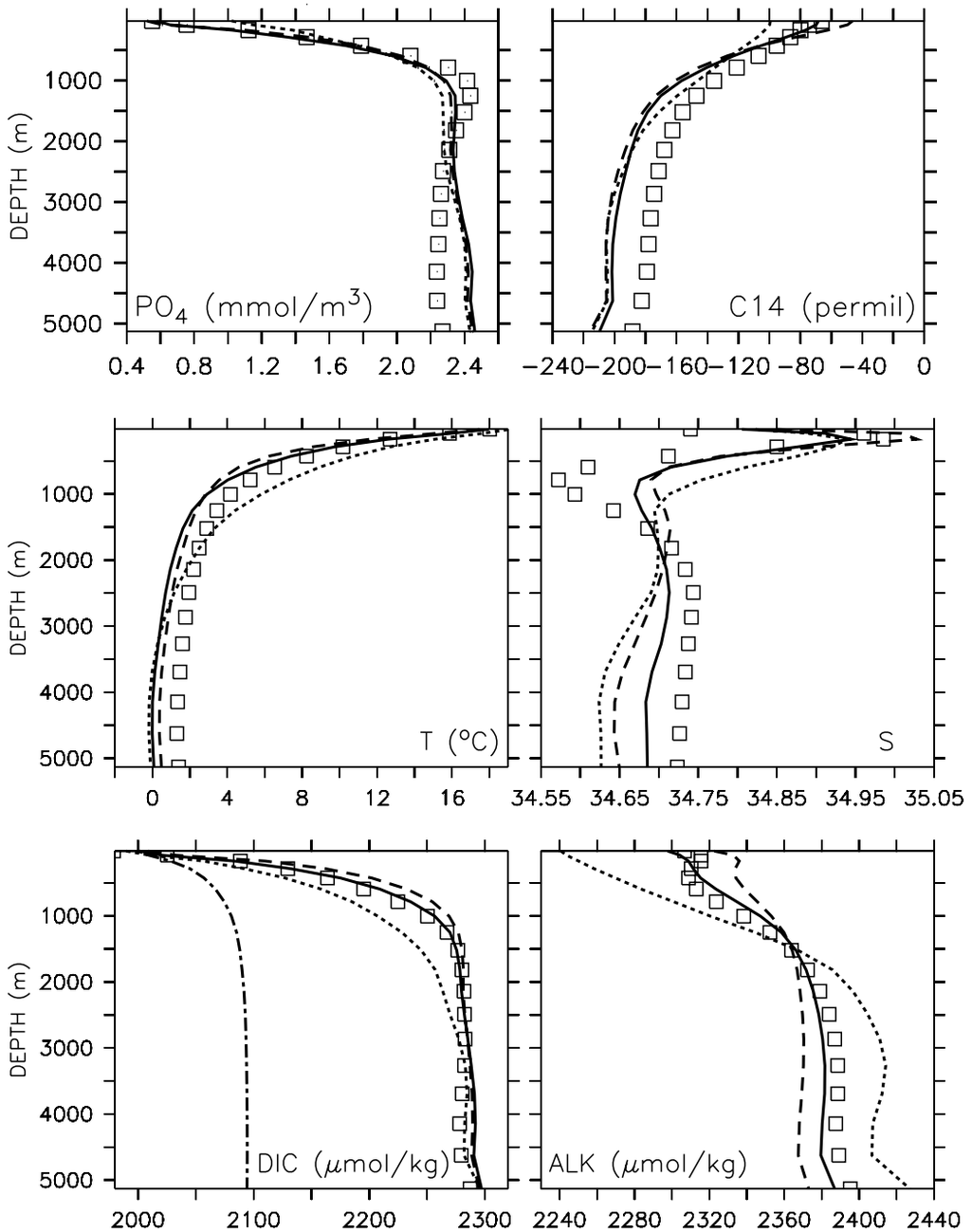

Figure 2. Globally horizontally averaged profiles of phosphate, natural radiocarbon, temperature, salinity, DIC and ALK. Symbols show present day observations from the World Ocean Atlas 2001 [*Conkright et al.*, 2002] and preindustrial estimates from GLODAP [*Key et al.*, 2004]. Solid line: present day control run (wNPs ctr), dashed line: 0.5 × WS, dotted line: 2 × WS. The dash-dotted line in the lower left panel shows the preindustrial DIC profile of the inorganic model (NoBio).

Table 1. Circulation indices from equilibrium experiments. Columns show the Antarctic Circumpolar Current (ACC) flow through Drake Passage (68°W), Indonesian Throughflow (ITF), Northern and Southern Tropical Ekman Cells (NTEC, STEC) computed as the maximum/minimum global streamfunction (vertically and zonally integrated meridional velocity) between 20°S-20°N, maximum of Overturning in North Atlantic (ONA) computed as the maximum streamfunction in the North Atlantic below 300m, export of North Atlantic Deep Water into the Southern Ocean (NADW) computed as maximum Atlantic streamfunction at 35°S below 300m, Overturning in North Pacific (ONP) computed as the maximum North Pacific streamfunction below 300m, CircumPolar Deep Water (CPDW) flux into Indo-Pacific computed as minimum Indo-Pacific streamfunction at 35°S below 300m, UpWelling in the Southern Ocean (UWSO) computed as the maximum streamfuction south of 35°S below 300m, Antarctic DownWelling (AADW) computed as the minimum streamfunction south of 60°S below 300m, globally integrated Antarctic Bottom Water (AABW) cell computed as the minimum streamfunction below 2000m.

Model Version	Experiment	ACC (Sv)	ITF (Sv)	NTEC (Sv)	STEC (Sv)	ONA (Sv)	NADW (Sv)	ONP (Sv)	CPDW (Sv)	UWSO (Sv)	AADW (Sv)	AABW (Sv)
wNPs	ctr	80	19	40	54	15	14	1	11	22	4	14
	0.5 × WS	54	13	22	28	12	10	2	12	7	3	14
	2 × WS	147	29	90	103	21	19	2	12	49	2	15
	NADW off	79	12	39	55	0	0	9	8	19	4	13
	NADW off + $\Delta\tau_{GENESIS}$	79	11	38	50	0	0	11	8	18	4	13
	Kv_{SO} = 1	71	19	39	49	18	17	0	12	21	3	9
	LGM ctr	88	17	41	54	13	11	2	9	21	7	14
	LGM NADW off	86	13	41	53	2	2	7	8	19	8	14
sNPs	ctr	80	20	40	54	17	16	0	12	22	3	12
	NADW off	84	14	38	56	0	0	2	8	17	3	13
	tidal off	83	17	40	52	15	14	0	8	22	3	9

Table 2. Global carbon and productivity results from equilibrium experiments. Columns show atmospheric CO_2 concentration; difference in atmospheric CO_2 from control run (ΔCO_2); changes in ocean (ΔC^O) and land (ΔC^L) carbon inventories; surface ocean partial pressure of CO_2 (P_{CO2}) over sea ice free area; changes in P_{CO2} (ΔP_{CO2}) can be separated into changes in solubility due redistributions of temperature and salinity ΔP_{CO2}(T,S) and changes involving biology due to redistributions of DIC and ALK ΔP_{CO2}(D,A). Export Production (EP) through sinking of particulate organic matter, New Production (NP), Net Primary Production (NPP)

Model Version	Experiment	CO_2 ppmv	ΔCO_2 ppmv	ΔC^O GtC	ΔC^L GtC	P_{CO2} ppmv	ΔP_{CO2} ppmv	ΔP_{CO2} (T,S) ppmv	ΔP_{CO2} (D,A) ppmv	EP GtC/yr	NP GtC/yr	NPP GtC/yr
wNPs	ctr	308	0	0	0	295	0	0	0	6.2	7.8	53
	0.5 × WS	284	–24	+109	–59	270	–25	–8	–20	5.0	6.0	41
	2 × WS	389	+81	–364	+194	380	+85	+22	+67	9.2	12	90
	NADW off	336	+27	–104	+46	322	+27	+8	+20	5.8	7.3	51
	NADW off + $\Delta\tau_{GENESIS}$	336	+27	–104	+45	322	+30	+9	+22	5.8	7.4	51
	Kv_{SO} = 1	326	+21	–89	+45	313	+21	+5	+17	7.1	8.8	61
	NoBio ctr	295	0	0	0	285	0	0	0	NA	NA	NA
	NoBio NADW off	290	–5	28	–16	278	–7	–1	–6	NA	NA	NA
	LGM ctr	281	0	0	0	261	0	0	0	5.5	6.9	40
	LGM NADW off	286	+5	–18	+8	266	+5	+1	+4	4.9	6.2	37
sNPs	ctr	308	0	0	0	298	0	0	0	6.2	7.8	50
	NADW off	332	+26	–71	+26	318	+20	+6	+15	5.6	7.2	50
	tidal off	286	–22	+103	–49	272	-26	-11	–18	5.4	6.9	46

impact on the ecosystem and its productivity (Table 2). New production increases by more than 50% and net primary production by about 70% in experiment 2 × WS compared with the control run. Surface nutrient concentrations increase and the nutricline weakens (Figure 2). Along with nutrients, carbon is shifted from the deep and intermediate ocean to the surface, where part of it escapes to the atmosphere. Surface ocean P_{CO2} changes are dominated by redistributions of DIC and ALK whereas changes due to T and S are smaller but not negligible (Table 2).

Atmospheric CO_2 levels are consequently higher the stronger the wind stress (Table 2), consistent with our working hypothesis. However, the response of CO_2 is nonlinear such that increasing the wind stress has a stronger effect than its reduction. The reason for this asymmetry is presumably related to the fact that surface nutrient concentrations are already very low in most parts of the tropical and subtropical oceans (globally averaged surface PO_4 is 0.55 mmol/m^3 in the observations and 0.58 in the wNPs control run). Thus reduced upwelling in experiment 0.5 × WS does not affect much nutrient concentrations in these waters and only leads to a small reduction in globally averaged surface phosphate to 0.52 mmol/m^3, whereas increased upwelling in run 2 × WS strongly increases surface nutrient concentrations everywhere to 1.0 mmol/m^3. This also explains the asymmetric response of productivity (Table 2). The strong increase in productivity and nutrient cycling in the surface layers in experiment 2 × WS also causes an acceleration of the carbonate pump (visible as the larger vertical gradient of alkalinity in Figure 2 since production of $CaCO_3$ is parameterized as a constant fraction of POM production. This mechanism contributes to the rise in P_{CO2} of surface waters and hence atmospheric CO_2.

BUOYANCY DRIVEN CIRCULATION

Simulating a Shutdown of the Atlantic Overturning

In order to investigate the role of the buoyancy driven ocean circulation on atmospheric CO_2 an experiment was performed, in which deep water formation in the North Atlantic was stopped abruptly through the application of a freshwater pulse (Figure 3). This experiment is motivated by the paleo record from the last glacial period, which, as discussed in the introduction, indicates that such large and abrupt changes in ocean circulation have indeed occurred and that they were related to variations in atmospheric CO_2 [*Indermühle et al*., 2000].

In response to the rapid reduction in ocean circulation atmospheric CO_2 increases gradually in our model on a multimillennial time scale. This is, at least at first glance, contrary to our working hypothesis. In the following we present a detailed analysis in order to better understand this unexpected model behavior. First we notice that the atmospheric CO_2 increase is caused by a reduction in the oceanic carbon inventory by more than 100 GtC (Figure 3, Table 2), whereas the terrestrial carbon pool acts as a buffer increasing by 46 GtC. Less than one third (14 GtC) of this increase is due to changes in the soil carbon pool whereas two thirds (32 GtC) are caused by vegetation carbon changes. Vegetation carbon declines in northern and central Europe and increases at low latitudes and around the North Pacific (Plate 1).

Decreased solubility due to slightly warmer sea surface temperatures contributes 8 ppmv (Table 2) to the total increase of surface water P_{CO2} of 27 ppmv, but the dominant factor in explaining the increase in atmospheric CO_2 is rather redistribution of DIC and ALK. The net changes in the oceanic carbon inventory are the result of much larger redistributions between the different ocean basins (Table 2, Figures 3 and 4). The large interbasin gradients of DIC and ALK in the control simulation are erased if NADW is stopped (Fig 4). Whereas the Atlantic inventory increases by almost 300 GtC, carbon storage in the other ocean basins declines. The largest reduction occurs in the Pacific with 340 GtC in model version wNPs and 289 GtC in model sNPs. The larger decrease in the Pacific carbon inventory in model wNPs is due to a shallow overturning circulation that develops in the North Pacific (Table 1) in response to the decrease of the Atlantic overturning consistent with the Atlantic-Pacific seesaw mechanism [*Saenko et al*., 2004]. This overturning, which is restricted to the northern hemisphere, removes carbon from the upper ocean in the North Pacific by downwelling of low nutrient, low carbon surface waters to intermediate depths of about 1500m. In model version sNPs subduction in the North Pacific is suppressed due to stronger stratification (Table 1) and thus the carbon loss from the Pacific is smaller.

In the abiotic run atmospheric CO_2 decreases slightly (by ~5 ppmv, Figure 3B, Table 2) and changes in the individual ocean basins are much smaller than in the full model (Table 3, thin lines in Figure 4). These results support the conclusion that changes in biologically mediated DIC and ALK are required to explain the full model response and that solubility changes play only a secondary role, contrary to the hypothesis of *Martin et al*. [2005].

Globally averaged DIC concentrations decrease below ~600m depth, with a maximum around 1300m (solid lines in Figure 5). This mid-depth maximum of depleted DIC concentrations is a robust feature in both model versions (wNPs and sNPs, not shown). Alkalinity shows a similar depletion around 1300m. Globally deep water freshens by 0.3 salinity units due to the missing injection of salty NADW, which also leads to a salinification of surface waters by ~0.2 units. Reduced upwelling of cold water into the thermocline allows

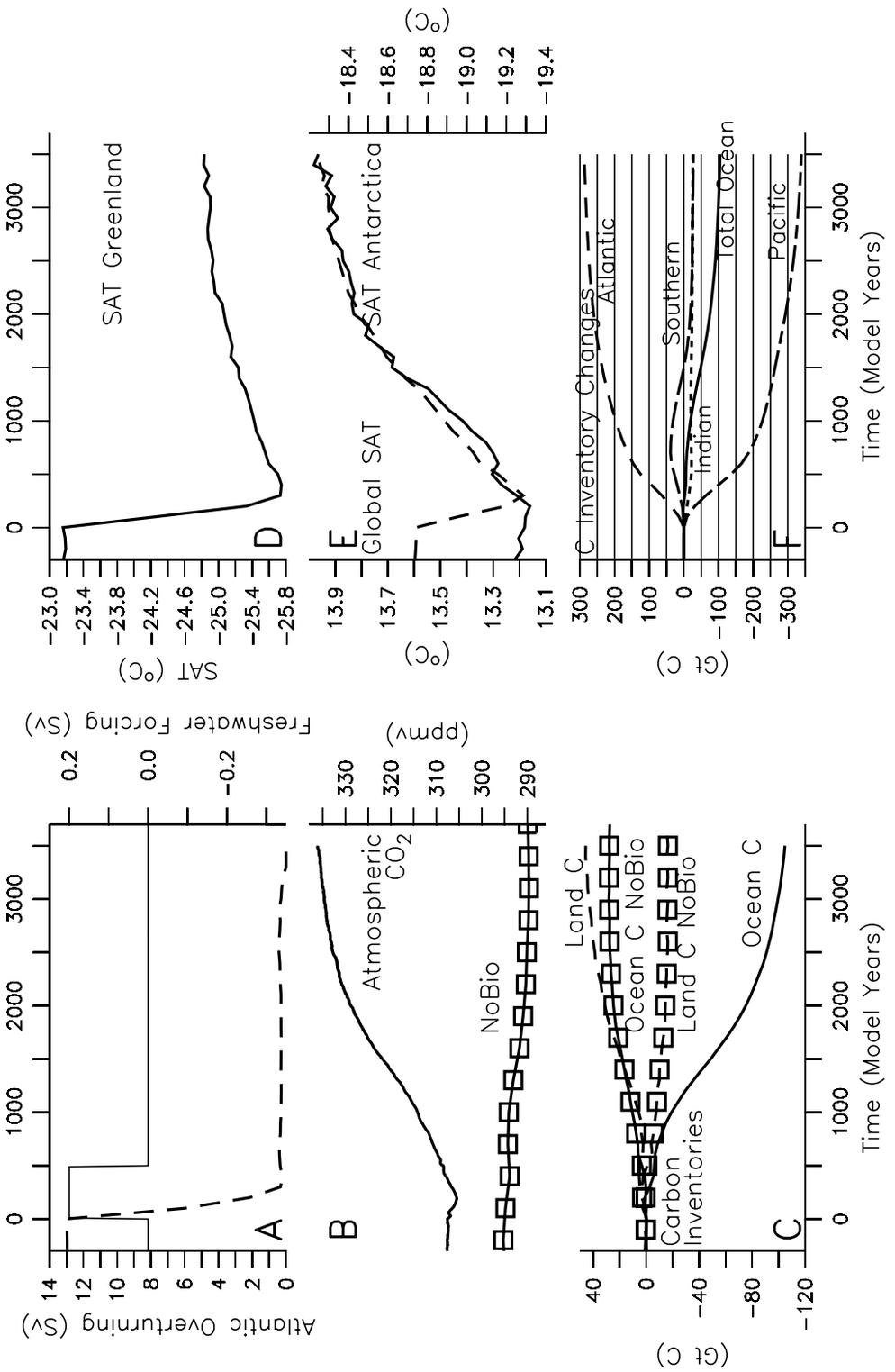

Figure 3. Transient model response to a shutdown of the Atlantic Overturning (dashed line in A) forced by a pulse of freshwater input to the North Atlantic (thin solid line in A). (B) Atmospheric CO_2 concentration. (C) Change in land and ocean carbon inventories. (D) Surface air temperature (SAT) in Greenland. (E) Global SAT (dashed, left scale) and SAT in Antarctica (solid, right scale). (F) Change in carbon inventories in the different ocean basins (Indian: dotted; Atlantic: short dashed; Pacific: short-long dashed; Southern Ocean: long dashed; Global: solid). Lines with square symbols in (B) and (C) represent the model version without ocean biology (NoBio)

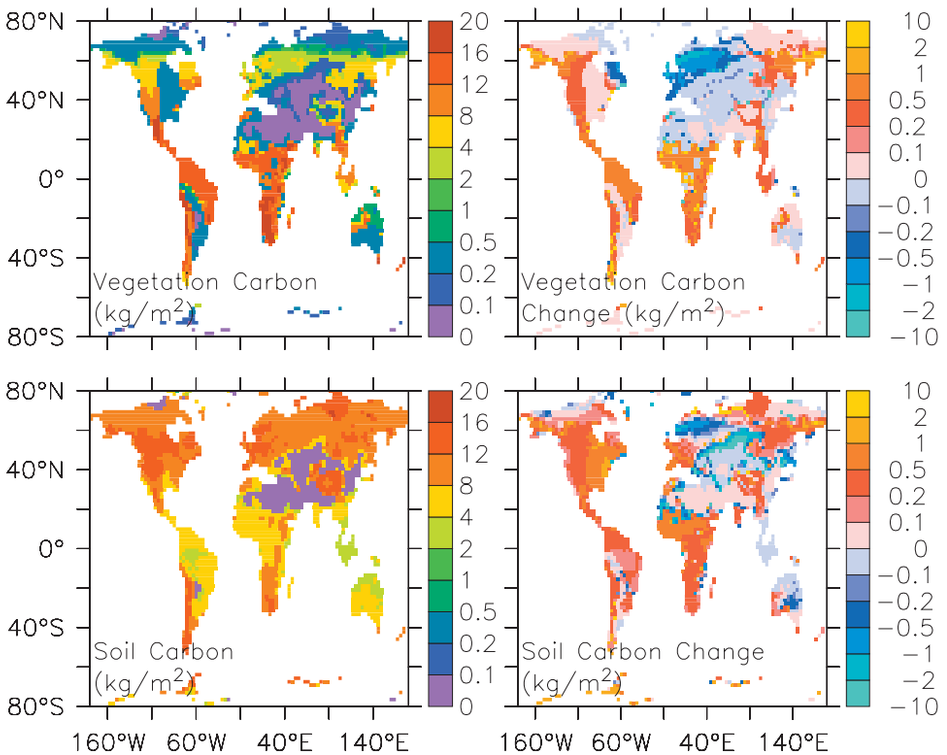

Plate 1. Vegetation (top) and soil (bottom) carbon pools in the preindustrial control simulation "wNPs ctr" (left panels) and their changes as a response to a permanent shutdown of the Atlantic overturning circulation ("wNPs NADW off" minus "wNPs ctr"; right panels).

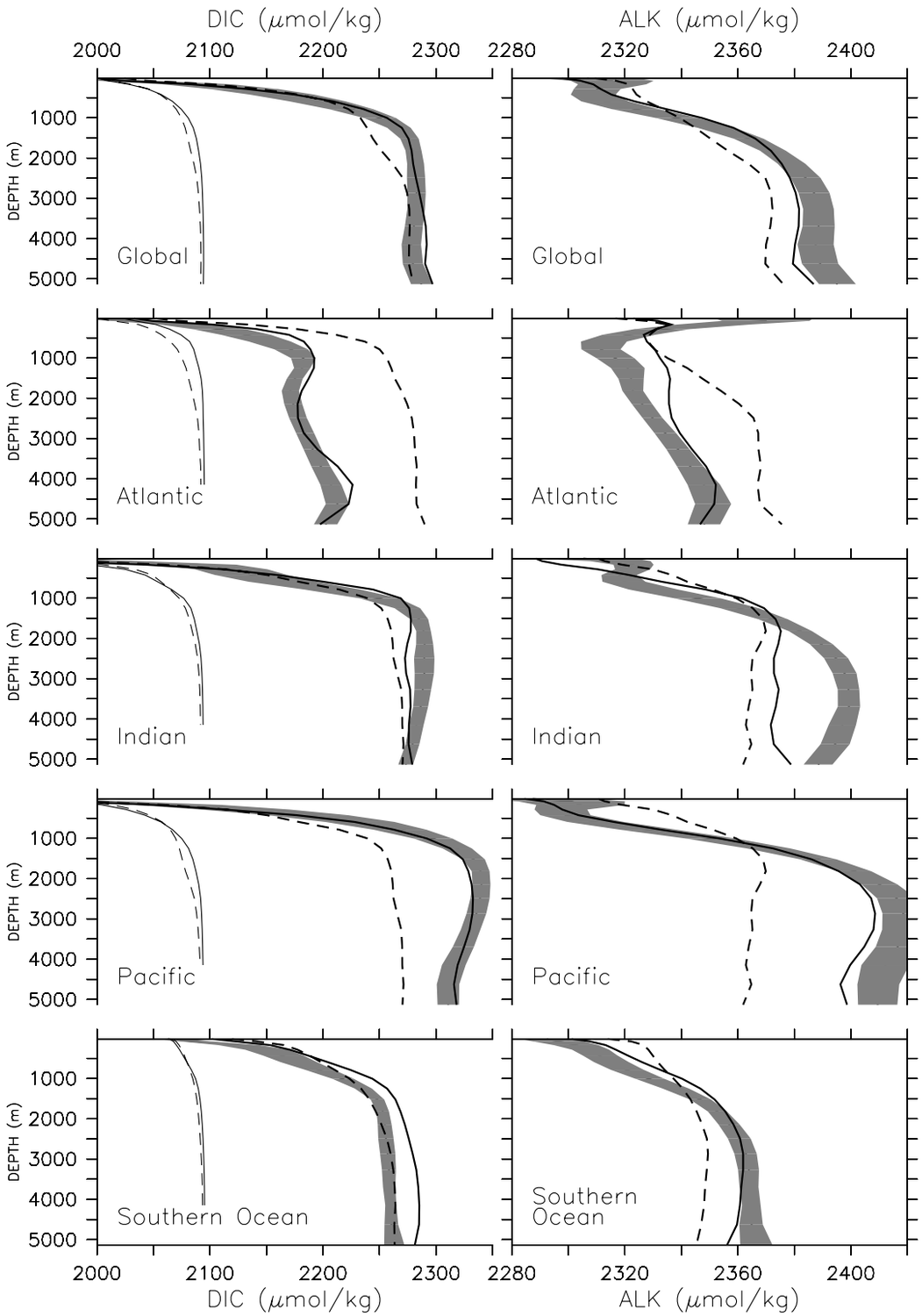

Figure 4. Basin wide averaged profiles of DIC (left) and ALK (right) versus depth. The thick solid line represents the control simulation "wNPs ctr" (year 0 in Figure 3), the thick dashed line the equilibrium without NADW formation "wNPs NADW off" (year 3700 in Figure 3). The Southern Ocean is defined south of 40°S. Thin lines show the corresponding profiles from the abiotic model version (NoBio). The gray shaded area shows observations with published error estimates (*Key et al*., 2004). In the case of DIC, anthropogenic CO_2 was subtracted to yield preindustrial values.

Table 3. Changes in ocean carbon inventory in the different ocean basins.

Model Version	Experiment	ΔC^O total	ΔC^O Atl.	ΔC^O Pac.	ΔC^O Ind.	ΔC^O SO
		GtC	GtC	GtC	GtC	GtC
wNPs	NADW off	–104	+288	–340	–26	–28
	NADW off + $\Delta\tau_{GENESIS}$	–104	+330	–379	–25	–31
	$Kv_{SO} = 1$	–89	+4	–22	–13	–58
	NoBio NADW off	+28	+46	–31	–2	+16
	LGM NADW off	–18	+170	–187	–6	+6
sNPs	NADW off	–79	+310	–289	–49	–52
	tidal off	+113	–23	+76	–4	+64

increased downward diffusion of heat at low latitudes and hence leads to warming of the upper ocean. Nutrient concentrations decrease in the upper 2 km and increase below. This is consistent with a vertical nutrient shift and reduced productivity associated with weaker deep water formation in the North Atlantic reported earlier [*Schmittner*, 2005].

Apparent oxygen utilization ($AOU = sat(O_2) - O_2$, the difference between the temperature dependent oxygen saturation and the in situ O_2 concentration), decreases in the deep ocean by up to 90 mmol/m^3. This corresponds to a ~30% reduction and is consistent with a decrease of the sinking and remineralization of POM into the deep ocean by a similar amplitude (not shown). This reduction of AOU implies a decrease of deep ocean remineralized phosphate ($P_r = AOU/R_{O:P}$, with $R_{O:P} = 208$ being the Redfield ratio of oxygen to phosphorus used in the model) by about 0.4 mmol/m^3. Using a carbon to phosphorus ratio of $R_{C:P} = 112$ this corresponds to a decrease of DIC by about 40 mmol/kg. Thus, the decrease of mid-depth carbon and phosphate concentrations can be attributed to a reduction of remineralized matter, whereas below 2 km depth larger increases in preformed nutrients $P_p = PO_4 - P_r$ (and carbon) dominate the inorganic tracer changes.

The surface to deep density difference decreases globally by about 0.2 kg/m^3, mainly due to the throttled subduction of relatively salty NADW to the deep ocean. In the Southern Ocean this is apparent by the absence of the tongue of high salinity NADW at mid depths (Plate 2) which leads to a large decrease in stratification (the average difference between surface and deep potential density south of 40°S decreases by ~25%, Figure 6) along with deepening of the surface mixed layer. Particularly around 58°S in the Pacific sector (not shown) maximum mixed layer depths increase dramatically tapping into the high DIC waters of the abyssal ocean. At this latitude the 27.6 σ_Θ isoline comes close to the surface in experiment "wNPs NADW off" (Plate 2). This isopycnal surface deepens at low latitudes to about 1500m. Thus, better ventilation of deep water around this potential density through steeper isopycnals and deeper mixed layers in the Southern Ocean around 58˚S provides a consistent explanation for the depletion of DIC concentrations around 1500m depth (Figure 5). The slow process of along isopycnal diffusion is also consistent with the long multi-millennial time scale of the simulated atmospheric CO_2 response.

Our analysis indicates that weakened stratification in the Southern Ocean is ultimately responsible for lower deep water DIC concentrations and higher atmospheric CO_2 in the simulations without NADW formation. This result is consistent with earlier studies emphasizing the importance of Southern Ocean ventilation on atmospheric CO_2 [*Siegenthaler and Wenk*, 1984; *Sarmiento and Toggweiler*, 1984; *Sarmiento and Orr*, 1991; *Toggweiler*, 1999; *Sigman and Boyle*, 2000; *Toggweiler et al*., 2006].

The simulated anti-phase behavior of stratification in the North Atlantic and Southern Ocean also supports the hypothesis of a bipolar seesaw of deep water formation suggested by *Broecker* [1998]. Deeper winter mixed layers result in increased heat loss to the atmosphere (not shown) and contribute to warming of the air at high southern latitudes thereby explaining the correlation between atmospheric CO_2 and air temperatures around Antarctica.

Comparison With the Paleo Record

The paleo record from Marine Isotope Stage 3 (MIS3, 30-60 ka BP) during the last ice age displays most clearly stadial to interstadial transitions (Figure 1), whereas rapid cooling (interstadial-stadial) events are not so unambiguously identifiable. Stadial-interstadial transitions are associated with rapid warmings of 8-15°C in Greenland [*Huber et al*., 2006], rapid increases in methane, and a resumption of the Atlantic overturning circulation. In order to improve comparison with the observations two additional model experiments were conducted that include stadial-interstadial transitions and differ in the duration of the stadial phase (Figure 7). The simulated temperature changes in Greenland are less than 5°C and clearly underestimated. Missing atmospheric dynamics and the coarse resolution might be responsible for this bias. Simulated atmospheric CO_2 raises gradually after the transition to the stadial phase. It peaks right at the stadial-interstadial transition and gradually decreases afterwards. The simulated atmospheric CO_2 changes are highly correlated with temperature changes over Antarctica with little or no time lag. All of these features are consistent with the observations (Figure 1).

The simulated amplitude of the CO_2 variations depends on the duration of the stadial phase. It is about 15 ppmv for a short

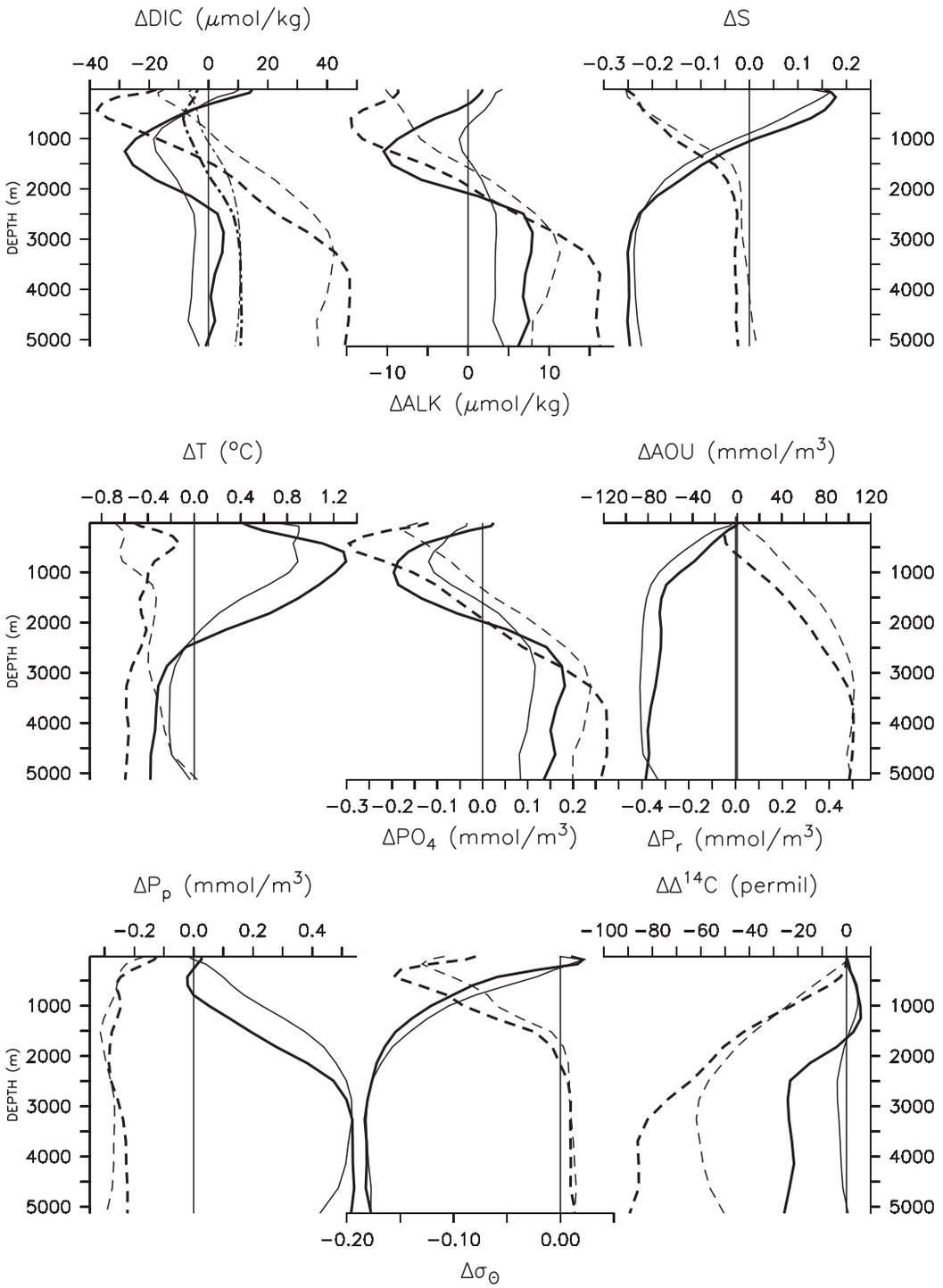

Figure 5. Globally averaged profiles of tracer changes caused by a cessation of NADW formation ("wNPs NADW off" minus "wNPs ctr", solid lines) or by removing tidal mixing ("sNPs tidal off" minus "sNPs ctr", dashed lines). Bold lines represent the global ocean, thin lines the Southern Ocean south of 40°S. DIC_m and ALK_m (mmol/m^3) anomalies do not include the effects of dilution (i.e. are not normalized with salinity in contrast to those shown in Plate 1) because dilution affects neither the global carbon inventory nor surface P_{CO2} and thus does not impact atmospheric CO_2. Dash-dotted lines in the top left panel show DIC anomalies due to a cessation of NADW formation in the inorganic model (NoBio).

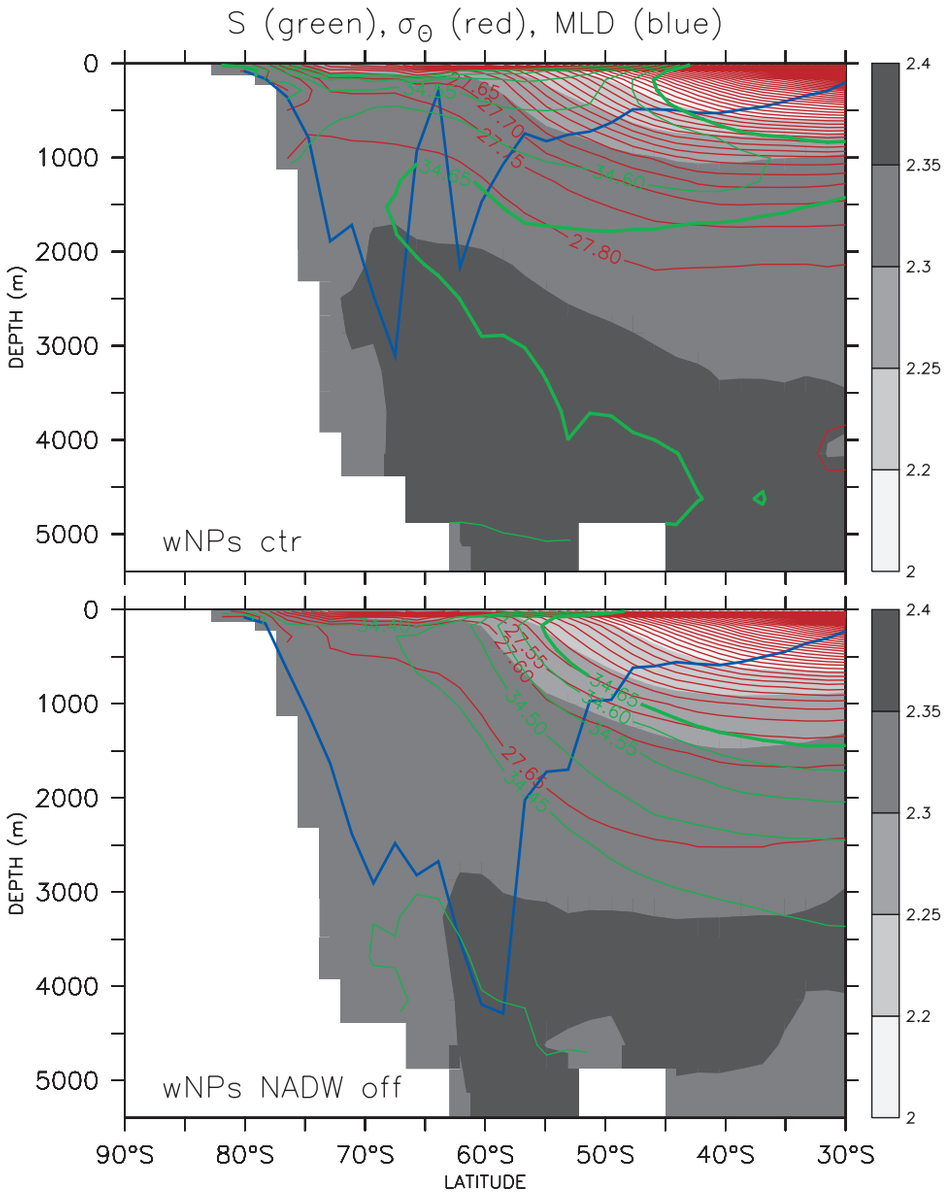

Plate 2. Zonally averaged DIC_m concentrations (mmol/m^3) in the Southern Ocean (gray shading), annual mean isopycnal surfaces (σ_Θ, red lines), salinity (green lines, the 34.65 isohaline is thicker), and zonal and monthly maximum of mixed layer depth (calculated as depth of 0.1 σ_Θ difference from surface layer, blue line).

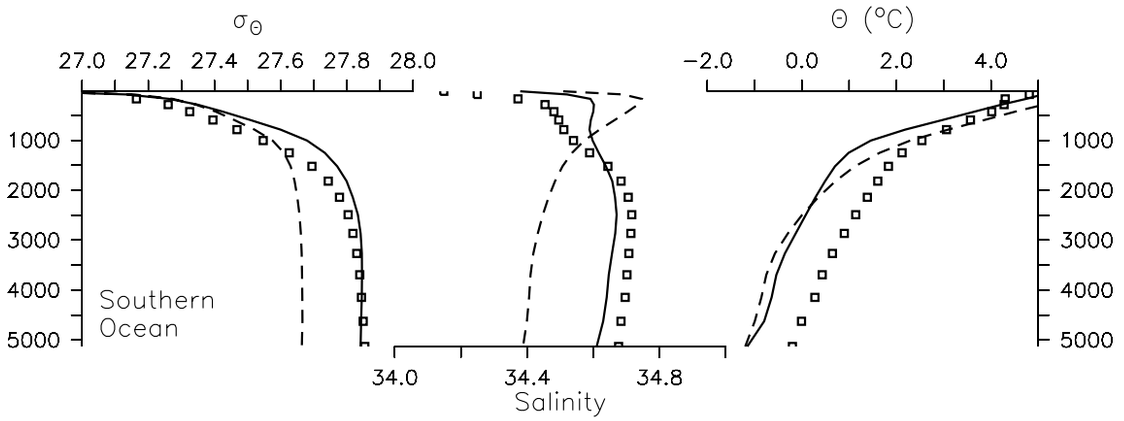

Figure 6. Depth profiles of potential density (left), salinity (center) and potential temperature (right) in the Southern Ocean for the control run ("wNPs ctr", solid lines), the equilibrium state without NADW formation ("wNPs NADW off", dashed lines) and present day observations [*Conkright et al*., 2002, symbols].

(1000 year long) stadial and almost double (30 ppmv) for a 2000 year long stadial. We hypothesize that this is due to the gradual nature of the CO_2 change, which does not reach equilibrium for short stadial durations. We propose this as an explanation of the lack of large high frequency variability in the observed CO_2 record. A stadial of less than 1000 year duration would have almost no appreciable atmospheric CO_2 signal owing to the sluggish response of the oceanic carbon cycle dominated by slow isopycnal diffusion.

A "Glacial" Simulation

All experiments described above were performed with a pre-industrial (interglacial) background climate. However, the climate during MIS3 was much different, with large ice sheets covering North America and Europe and a cooler and dryer atmosphere in general. As a first idealized test of the robustness of our model results with respect to the background climate, additional experiments have been conducted within a colder climatic state. A perturbation of 2.5 W/m^2 has been added permanently to the outgoing longwave radiation at the top-of-the-atmosphere which leads to a global cooling of surface air temperatures by 3°C. This corresponds approximately to conditions during the Last Glacial Maximum (LGM). This simulation is termed LGM ctr in Tables 1 and 2. However, no other changes (such as imposing ice sheets or lowering sea level) have been made, and as such this experiment does not represent a realistic glacial climate but rather an idealized sensitivity experiment. Note also that atmospheric CO_2 is still at an interglacial level of 280 ppmv in this experiment. Obviously the model is unable to simulate the observed glacial-interglacial CO_2 change of ~80-100 ppmv. However, in this paper we are not concerned with the glacial-interglacial CO_2 problem, which remains unsolved.

The export of North Atlantic Deep Water to the Southern Ocean is reduced by more than 20% in the LGM ctr run (Table 1) and downwelling along Antarctica is increased due to enhanced sea ice formation. Both features have already been reported in earlier glacial studies with the same model [*Weaver et al*., 1998; *Schmittner*, 2003]. The response of atmospheric CO_2 to a shutdown of NADW formation (experiment "LGM NADW off") is strongly reduced from 27 ppmv in the preindustrial model to only 5 ppmv (Table 2). Redistribution of carbon between the different ocean basins is qualitatively similar to the interglacial model version (Table 2) in that it shows a large increase in the Atlantic and a decrease in the Pacific; however, the magnitude is much smaller. Inspection of the vertical changes (not shown) also reveals qualitatively similar results to the interglacial model (e.g. the maximum decrease of DIC around 1300m depth in Figure 6) but with reduced amplitudes.

These results suggest that the responses of the oceanic carbon cycle and atmospheric CO_2 are sensitive to the background climate, presumably owing to the weaker mean state of the Atlantic overturning in the LGM ctr run. This reduces the effect of NADW on the stratification in the Southern Ocean and leads to a muted response if NADW is shut off. The observed amplitude of atmospheric CO_2 changes of ~15 ppmv (Figure 1) during MIS3 is between the amplitude in the interglacial (27 ppmv) and the full glacial (5 ppmv) model simulations and as such it is not inconsistent with our model simulations.

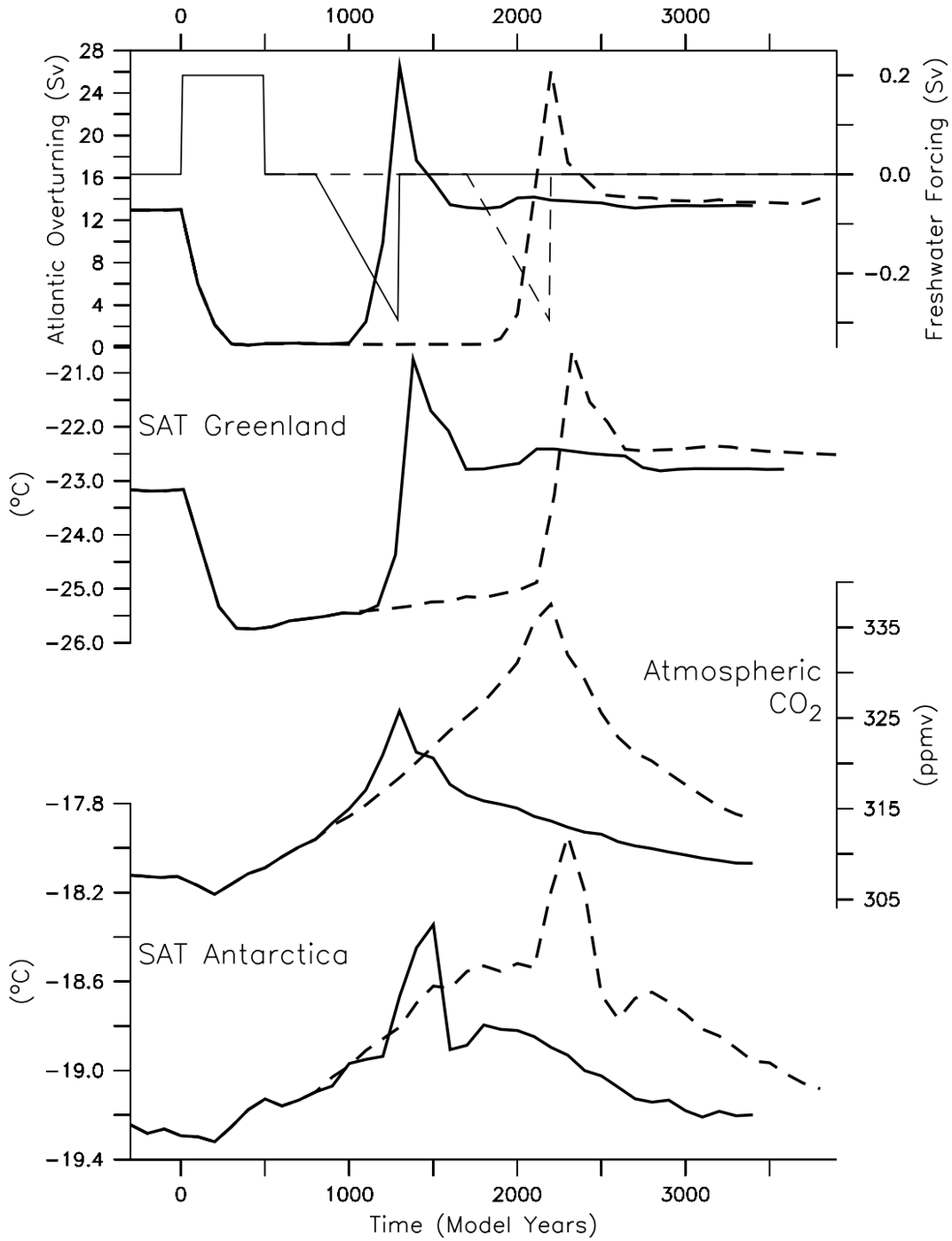

Figure 7. Response of atmospheric CO_2 (second panel from below) and SATs in Greenland (second panel from above) and Antarctica (bottom panel) to a collapse of the Atlantic overturning (thick lines in top panel) at year 0 and its resumption after 1000 years (solid lines) and 2000 years (dashed lines). Thin lines in top panel denote the freshwater forcing.

Additional Sensitivity Experiments

Influence of wind changes. In order to quantify the effect of wind driven ocean circulation changes brought about by the response of atmospheric dynamics to the shutdown of the Atlantic overturning circulation offline simulations with the GENESIS atmospheric General Circulation Model (GCM) have been conducted using SST and sea ice boundary conditions from the UVic model runs "wNPs ctr" and "wNPs NADW off". Resulting wind stress anomalies have been used to force an experiment otherwise equivalent to 'wNPs NADW off". This experiment is labeled "wNPs NADW off + $\Delta\tau_{\text{GENESIS}}$" in Tables 1 and 2. The resulting wind stress anomalies and a more detailed description of the method as well as its effect on subsurface oxygen concentrations is described elsewhere (*Schmittner et al*., submitted manuscript). The resulting changes in the wind driven circulation have no effect on atmospheric CO_2 as evident by an unchanged equilibrium concentration (Table 2) and almost identical transient CO_2 changes (not shown).

Effect of Southern Ocean stratification. In order to further explore the effect of Southern Ocean stratification on atmospheric CO_2 concentrations we performed two additional simulations. In the first experiment the enhancement of diapycnal mixing due to tidally induced energy dissipation over rough topography was set to zero everywhere in the ocean. In this experiment (called "tidal off" in Tables 1 and 2) the diapycnal diffusivity is constant everywhere and equal to its background value ($K_v = K_b = 2 \times 10^{-5} m^2/s$). The simulated circulation changes are consistent with earlier results [*Saenko and Merryfield*, 2005] in that the global Antarctic Bottom Water cell is strongly reduced in strength, less Circumpolar Deep Water enters the Pacific, but the overturning in the Atlantic is only marginally weaker (Table 1). Reduced topographically enhanced mixing in the Southern Ocean leads to increased stratification there (see dashed lines in Figure 5) and lower atmospheric CO_2 by 22 ppmv.

Decreased ventilation of the deep ocean leads to older surface to deep radiocarbon age differences. Globally the surface to deep $\Delta^{14}C$ gradient increases by 100 permil. Reduced nutrient delivery to Southern Ocean surface waters leads to a decrease of global productivity and export of POM. However, despite slightly reduced remineralization of POM in the deep ocean (by ~10%, not shown) AOU increases, indicating higher concentrations of remineralized nutrients P_r in the deep sea. Thus, we conclude that these higher remineralized nutrient concentrations result from reduced removal of these nutrients from the deep sea by weaker ventilation.

In a second experiment the vertical diffusivity in the Southern Ocean south of 40°S and below 500m depth has been set to a minimum of 1 cm^2/s ("$K_v^{SO} = 1$" in Tables 1 and 2) in accordance with present day observations [*Naveira Garabato et al*., 2004; *Sloyan*, 2005] which show larger background values than our default model. The reason for the higher background diffusivities in the Southern Ocean is not clear but might be related to interaction of the ACC with the rough topography [*Sloyan*, 2005], an effect not considered in the tidal mixing scheme. Anyway, increased mixing in the Southern Ocean only weakens stratification there and leads to an increased overturning in the North Atlantic (Table 1). Atmospheric CO_2 increases by 21 ppmv (Table 2). Both experiments demonstrate that stratification in the Southern Ocean is important in controlling atmospheric CO_2 and not the Atlantic overturning circulation itself. Adding the effect of enhanced mixing due to tides and that of increased background mixing, the total effect of enhanced mixing in the present day Southern Ocean leads to more than 40 ppmv higher atmospheric CO_2 concentrations. A more detailed description of the tracer distributions in these experiments is planned elsewhere.

DISCUSSION AND CONCLUSIONS

Our model simulations suggest that changes in both wind and buoyancy driven ocean circulation can have a large impact on atmospheric CO_2 concentrations. Results from transient simulations with large and rapid changes of the Atlantic overturning circulation are consistent with a number of characteristics in the glacial ice core record. After an abrupt collapse of the overturning, atmospheric CO_2 slowly increases by more than 20 ppmv on a multi-millennial time scale. This time scale is set by the slow equilibration of the deep ocean through along isopycnal mixing processes. Therefore, higher frequency (centennial) oscillations of the overturning excite no measurable response in atmospheric CO_2 and the amplitude of the CO_2 variation is larger for longer period oscillations.

Simulated Antarctic temperatures and atmospheric CO_2 peak at the time of rapid resumption of the circulation and gradually decline afterwards. Changes in stratification in the Southern Ocean are the key process that controls atmospheric CO_2 and not the overturning itself. However, resumption of the Atlantic overturning and associated injection of salty NADW increases stratification in the Southern Ocean, leading to declining CO_2, less heat loss to high southern latitude surface waters during winter and hence cooler air temperatures over Antarctica. These model results are qualitatively and quantitatively consistent with observations from the glacial ice core CO_2 record (Figure 1) and provide an explanation for their gradual changes and low frequency variability.

The simulated CO_2 response is sensitive to the model background climate and larger in amplitude in a warmer climate with a stronger interstadial overturning circulation. More work is needed to perform experiments with a more realistic

background state of glacial climate and carbon cycle including a realistic ice sheet cover. The latter has been shown to be important for the response of the terrestrial carbon inventory [*Köhler et al*., 2005b].

Other more idealized experiments suggest that the observed enhancement of vertical mixing over rough topography in the Southern Ocean leads to higher atmospheric CO_2 by ~40 ppmv, confirming the sensitivity of atmospheric CO_2 to processes that affect stratification in Antarctic waters. The sensitivity of CO_2 to mixing in the Southern Ocean also calls for intensified efforts to develop, improve and implement process based parameterizations of mixing in ocean climate models. We have shown how enhanced mixing over rough topography in the Southern Ocean affects stratification there and hence atmospheric CO_2. We recommend the tidal mixing parameterization [*Simmons et al*., 2004] to be used also in other ocean climate models, particularly if used for biogeochemical studies. So far most models still use more simplified schemes. The coupled Geophysical Fluid Dynamics Laboratory model CM2, for example, uses the constant vertical profile of *Bryan and Lewis* [1979] mimicking bottom intensified mixing [*Gnanadesikan et al*., 2006]. However, other processes that lead to enhanced mixing, e.g. the interaction of the barotropic flow with rough topography in the Southern Ocean [*Sloyan*, 2005], wind induced turbulence, or the effects of tropical cyclones on mixing in the low latitude thermocline [*Emanuel*, 2001] are much less understood and more basic research will be needed before parameterisations for GCMs can be developed.

Our results appear to contrast with those of *Köhler et al*. [2005b] after which changes in the terrestrial carbon inventory cause an increase of atmospheric CO_2 after a collapse of the Atlantic overturning. We can neither support the suggestion by *Martin et al*. [2005] after which solubility alone could explain the multi-millennial glacial CO_2 variations. Our results are also in contrast to box model and other more simplified model simulations that show lower atmospheric CO_2 in response to decreased overturning circulation [*Keir*, 1988; *Heinze and Hasselmann*, 1993; *Schulz et al*., 2001; *Cameron et al*., 2005; *Köhler et al*., 2005a, 2006]. The reason for this discrepancy might be related to the fact that box models or other simplified models do not capture the effect of NADW on Southern Ocean stratification and sea ice. Our results are consistent with and support the findings of *Marchal et al*. [1998, 1999], after which atmospheric CO_2 increases after a shutdown of the Atlantic overturning due to changes in ocean carbon cycling. However, here we attribute the reason for the CO_2 increase to changes in Southern Ocean stratification such as deeper mixed layers and steepening of isopycnals, whereas *Marchal et al*. [1998, 1999] emphasize solubility changes.

Our working hypothesis, after which a stronger ocean circulation leads to higher atmospheric CO_2, is apparently in conflict with the model response of higher CO_2 due to a collapsed Atlantic overturning circulation. Obviously this hypothesis is much too simplistic to apply to the real world or even the less complex model, but it might be reconciled with the model results if the term "ocean circulation" refers not only (or not mainly) to the large scale overturning circulation but rather also includes vertical mixing processes in the Southern Ocean which strongly control atmospheric CO_2. In response to a reduction of deep water formation in the North Atlantic, ventilation of deep and intermediate waters increases in the other two high latitude areas of the world ocean, the North Pacific and the Southern Ocean, supporting the ideas of *Broecker* [1998] and *Saenko et al*. [2004]. It appears as if the renewal of global deep and intermediate waters is resilient to perturbations and that a reduction in one of the three deep water formation regions will be compensated in the other regions. Here we have shown that this can lead to reduced carbon content in the ocean as a whole.

Acknowledgments. This research has been supported by the NSF Paleoclimate Program as part of the PaleoVar project.

REFERENCES

Ahn, J., and E.J. Brook, Atmospheric CO_2 and climate from 65 to 30 ka B.P., *Geophys. Res. Lett*., 34, L10703, doi:10.1029/2007GL029551, 2007.

Blunier, T., and E.J. Brook, Timing of millennial-scale climate change in Antarctica and Greenland during the last glacial period, *Science*, 291, 109-112, 2001.

Broecker, W.S., D.M. Petit, and D. Rind, Does the ocean-atmosphere system have more than one stable mode of operation? *Nature*, 315, 21-26, doi:10.1038/315021a0, 1985.

Broecker, W.S., Paleocean circulation during the last deglaciation: A bipolar seesaw? *Paleoceanogr*., 13, 119-121, 1998.

Brook, E.J., S. Harder, J. Severinghaus, E.J. Steig, and C.M. Sucher, On the origin and timing of rapid changes in atmospheric methane during the last glacial period, *Global Biogeochemical Cycles*, 14, 559-572, 2000.

Bryan, K., and L.J. Lewis, A water mass model of the world oceans, *J. Geophys. Res*., 84, 2503-2517, 1979.

Cameron, D.R., T.M. Lenton, A.J. Ridgwell, J.G. Shepherd, R. Marsh, and A. Yool, A factorial analysis of the marine carbon cycle and ocean circulation controls on atmospheric CO_2, *Global Biogeochem. Cycles*, 19, GB4027, doi:10.1029/2005GB002489.

Conkright, M.E. et al. World Ocean Database 2001, Volume 1: Introduction. Edited by S. Levitus, NOAA Atlas NESDIS 42, U.S. *Government Printing Office*, 167 pp., 2002.

Emanuel, K., Contribution of tropical cyclones to meridional heat transport by the oceans, *J. Geophys. Res*., 106, 14,771-14,781, 2001.

EPICA Community Members, One-to-one coupling of glacial climate variability in Greenland and Antarctica, *Nature*, 444, 195-198, 2006.

Ewen, T.L., A.J. Weaver, M. Eby, Sensitivity of the Inorganic Ocean Carbon Cycle to Future Climate Warming in the UVic Coupled Model, *Atmos.-Ocean*, 42, 23-42, 2004.

Ganachaud, A. and C. Wunsch, Improved estimates of global ocean circulation, heat transport and mixing from hydrographic data, *Nature*, 408, 453-457, 2000.

Ganeshram, R.S., S.E. Calvert, T.F. Pedersen and G.A. Cowie, Factors controlling the burial of organic carbon in laminated and bioturbated sediments off NW Mexico: Implications for hydrocarbon preservation. Geochim. *Cosmochim. Acta* 63, 1723-1734, 1999.

Gent, P.R., and J.C. McWilliams, Isopycnal mixing in ocean circulation models, *J. Phys. Oceanogr*., 20, 150-155, 1990.

Gnanadesikan, A. et al., GFDL's CM2 Global coupled climate models. Part II: The baseline ocean simulation, *J. Clim*., 19, 675-697, 2006.

Grootes, P.M., M. Stuiver, J.W.C. White, S.J. Johnsen, and J. Jouzel, Comparison of oxygen isotope records from the GISP2 and GRIP Greenland ice cores, *Nature*, 366, 552-554, 1993.

Heinze, C., and K. Hasselmann, Inverse multiparameter modeling of paleoclimate carbon cycle indices, *Quaternary Res*., 40, 281-296, 1993.

Huber, C., M. Leuenberger, R. Spahni, J. Flueckiger, J. Schwander, T.F. Stocker, S. Johnson, A. Landais, and J. Jouzel, Isotope calibrated Greenland temperature record over Marine Isotope Stage 3 and its relation to CH_4, *Earth and Planet. Sci. Let*., 243, 504-519, 2006.

Indermühle, A., E. Monnin, B. Stauffer, T.F. Stocker, and M. Wahlen, Atmospheric CO_2 concentration from 60 to 20 kyr BP from the Taylor Dome ice core, Antarctica, *Geophys. Res. Lett*., 27, 735-738, 2000.

Jaccard, S.L., G.H. Haug, D.M. Sigman, T.F. Pedersen, H.R. Thierstein, and U. Röhl, Science, 308, 1003-1006, 2005.

Johnsen, S.J., W. Dansgaard, H.B. Clausen, and C.C. Langway Jr., Oxygen isotope profiles through the Antarctic and Greenland ice sheets, *Nature*, 235, 429, 1972.

Key, R.M. et al., A global ocean carbon climatology: Results from GLODAP, Glob. Biogeochem. *Cycles*, 18, GB4031, 2004.

Keigwin, L.D., Glacial-age hydrography of the far Northwestern Pacific Ocean, Paleoceanogr., 13, 323-339, 1998.

Keir, R.S., On the late Pleistocene ocean chemistry and circulation, *Paleoceanogr*., 3, 413-445, 1988.

Köhler, P., H. Fischer, G. Munhoven, and R.E. Zeebe, Quantitative interpretation of atmospheric carbon records over the last glacial termination, Global Biogeochem. *Cycles*, 19, GB4020, doi:10.1029/2004GB002345, 2005a.

Köhler, P., F. Joos, S. Gerber, and R. Knutti, Simulated changes in vegetation distribution, land carbon storage, and atmospheric CO_2 in response to a collapse of the North Atlantic thermohaline circulation, *Clim. Dyn*., 25, 689-708, 2005b.

Köhler, P., R. Muscheler, H. Fischer, A model-based interpretation of low-frequency changes in the carbon cycle during the last 120,000 years and its implications for the reconstruction of atmospheric $\Delta^{14}C$, Geochem. *Geophys. Geosys*., 7, Q11N06, doi:10.1029/2005GC001228, 2006.

Matsumoto, K. et al., Evaluation of ocean carbon cycle models with data-based metrics, *Geophys. Res. Lett*., 31, L07303, doi:10.1029/2003GL018970, 2004.

Marchal, O., T.F. Stocker, and F. Joos, Impact of oceanic reorganizations on the ocean carbon cycle and atmospheric carbon dioxide content, *Paleoceanogr*., 13, 225-244, 1998.

Marchal, O., T.F. Stocker, J. Joos, A. Indermühle, T. Blunier, and J. Tschumi, Modelling the concentration of atmospheric CO2 during the Younger Dryas climate event, *Clim. Dyn*., 15, 341- 354, 1999.

Martin, P., D. Archer, and D.W. Lea, Role of deep sea temperature in the carbon cycle during the last glacial, *Paleoceanogr*., 20, PA2015, doi:10.1029/2003PA000914, 2005.

McPhaden, M.J., and D. Zhang, Slowdown of the meridional overturning circulation in the upper Pacific Ocean, *Nature*, 415, 603-608, 2002.

Meissner, K.J., A.J. Weaver, H.D. Matthews and P.M. Cox, The role of land surface dynamics in glacial inception: a study with the UVic Earth System Model, *Clim. Dyn*., 21, 515-537, 2003.

Naveira Garabato, A.C., K.L. Polzin, B.A. King, K.J. Heywood, and M. Visbeck, Widespread Intense Turbulent Mixing in the Southern Ocean, *Science*, 303, 210-213, 2004.

Neftel, A., H. Oeschger, T. Stauffelbach, and B. Stauffer, CO_2 record in the Byrd ice core 50,000-5000 years BP, *Nature*, 331, 609-611, 1988.

Orr, J.C., Najjar, R., Sabine, C.L., Joos, and F., Abiotic-HOWTO, Internal OCMIP Report, LSCE/CEA Saclay, Gif-sur-Yvette, *France*, 25pp., 1999.

Rashid, H., R. Hesse, and D.J.W. Piper, Evidence for an additional Heinrich event between H5 and H6 in the Labrador Sea, Paleoceanogr., 18, doi:10.1029/2003PA000913, 2003.

Saenko, O.A., A. Schmittner, and A.J. Weaver, On the Role of Wind-Driven Sea Ice Motion on Ocean Ventilation, *J. Phys. Oceanogr*., 32, 3376-3395, 2002.

Saenko, O.A., A. Schmittner, and A.J. Weaver, The Atlantic-Pacific Seesaw, *J. Clim*., 17, 2033-2038, 2004.

Saenko, O.A., and W.J. Merryfield, On the effect of topographically enhanced mixing on the global ocean circulation, *J. Phys. Oceanogr*., 35, 826-834, 2005.

Sarmiento, J.L., and J.R. Toggweiler, A new model for the role of the oceans in determining atmospheric P_{CO2}, *Nature*, 308, 621-624, 1984.

Sarmiento, J.L. and J.C. Orr, Three-dimensional simulations of the impact of Southern Ocean nutrient depletion on atmospheric CO_2 and ocean chemistry, *Limnol. Oceanogr*., 36, 1928-1950, 1991.

Sarmiento, J.L., Dunne, J., Gnanadesikan, A., Key, R.M., Matsumoto, K., Slater, R., A new estimate of the $CaCO_3$ to organic carbon export ratio, *Glob. Biogeochem. Cycles*, 1107, doi:10.1029/2002GB001919, 2002.

Sarmiento, J.L. and N. Gruber, Ocean Biogeochemical Dynamics, Princeton University Press, *Princeton*, N.J., 2006.

Sarnthein, M., K. Stattegger, D. Dreger, H. Erlenkeuser, P. Grootes, B.J. Haupt, S. Jung, T. Kiefer, W. Kuhnt, U. Pflaumann, C. Schäfer-Neth, H. Schulz, M. Schulz, D. Seidov, J. Simstich, S. van Kreveld, E. Vogelsang, A. Völker, and M. Weinelt (2001), Fundamental modes and abrupt changes in North Atlantic circulation and climate over the last 60 ky – concepts, reconstruction and numerical modeling, in The Northern North Atlantic: A Changing Envrionment, edited by P. Schäfer, M. Schlüter, W. Ritzrau, and *J. Thiede*, pp. 356-410, Springer-Verlag, Berlin.

Schartau, M., and A. Oschlies, Simultaneous data-based optimization of a 1D-ecosystem model at three locations in the North Atlantic: Part I-Method and parameter estimates, *J. Mar. Res*., 61, 765-793, 2003.

Schmittner, A., and A.C. Clement, Sensitivity of the thermohaline circulation to tropical and high latitude freshwater forcing during the last glacial-interglacial cycle, *Paleoceanogr*., 17, doi:10.1029/2000PA000591, 2002.

Schmittner, A., Yoshimori, M. and Weaver, A.J., Instability of glacial climate in a model of the ocean-atmosphere-cryosphere system, *Science*, 295, 1489-1493, 2002.

Schmittner, A., O.A. Saenko, and A.J. Weaver, Coupling of the hemispheres in observations and simulations of glacial climate change, *Quat. Sci. Rev*., 22, 659-671, doi:10.1016/S0277-3791(02)00184-1, 2003.

Schmittner, A., Southern Ocean sea ice and radiocarbon ages of glacial bottom waters, *Earth and Planet. Sci. Let*., 213, 53-62, doi:10.1016/S0012-821X(03)00291-7, 2003.

Schmittner, A., A. Oschlies, X. Giraud, M. Eby, H.L. Simmons, A global model of the marine ecosystem for long-term simulations: Sensitivity to ocean mixing, buoyancy forcing, particle sinking, and dissolved organic matter cycling, *Glob. Biogeochem. Cycles*, 19, GB3004, 2005.

Schmittner, A., Decline of the marine ecosystem caused by a reduction in the Atlantic overturning circulation, *Nature*, 434, 628-633, 2005.

Schmittner, A., E.D. Galbraith, S.W. Hostetler and T.F. Pedersen, Large fluctuations of dissolved oxygen in the Indian and Pacific oceans during Dansgaard/Oeschger oscillations caused by variations of North Atlantic Deep Water Subduction, Paleoceanography, in press.

Schmittner, A., A. Oschlies, H.D. Matthews and E.D. Galbraith, Future changes in climate, ocean circulation, ecosystems and biogeochemical cycling simulated for a business-as-usual CO_2 emission scenario until year 4000 AD, *Global Biogeochem. Cycles*, submitted.

Scholze, M., W. Knorr and M. Heimann, Modelling terrestrial vegetation dynamics and carbon cycling for an abrupt climate change event, *Holocene*, 13, 327-333, 2003.

Siegenthaler, U. and Th. Wenk, Rapid atmospheric CO_2 variations and ocean circulation, *Nature*, 308, 624-626, 1984.

Sigman, D.M., and E.A. Boyle, Glacial/interglacial variations in atmospheric carbon dioxide, *Nature*, 407, 859-869, 2000.

Simmons, H.L., S.R. Jayne, L.C. St. Laurent, and A.J. Weaver, Tidally driven mixing in a numerical model of the ocean general circulation, *Ocean Modell*., 6, 245– 263, 2004.

Sloyan, B.M., Spatial variability of mixing in the Southern Ocean, *Geophys. Res. Let*., 32, L18603, doi:10.1029/2005GL023568, 2005.

Toggweiler, J.R. and Samuels, B., Effect of Drake Passage on the global thermohaline circulation, *Deep-Sea Res*., 42, 477-500, 1995.

Toggweiler, J.R., Variation of atmospheric CO_2 by ventilation of the ocean's deepest water, *Paleoceanogr*., 14, 571-588, 1999.

Toggweiler, J.R., A. Gnanadesikan, S. Carson, R. Murnane, and J.L. Sarmiento, Representation of the carbon cycle in box models and GCMs: 1. Solubility pump, Global Biogeochem. *Cycles*, 17, 1026, doi:10.1029/2001GB001401, 2003.

Toggweiler, J.R., J.L. Russell and S.R. Carson, Midlatitude westerlies, atmospheric CO_2, and climate change during the ice ages, *Paleoceanogr*, 21, PA2005, doi:10.1029/2005PA001154, 2006.

Weaver, A.J., M. Eby, A.F. Fanning and E.C. Wiebe, Simulated influence of carbon dioxide, orbital forcing and ice sheets on the climate of the last glacial maximum, *Nature*, 394, 847-853, 1998.

Weaver, A.J., et al., The UVic Earth System Climate Model: Model description, climatology, and applications to past, present and future climates, *Atmos. Ocean*, 39(4), 361–428, 2001.

J. Ahn and E. J. Brook, Department of Geosciences, Oregon State University, Corvallis, Oregon, USA.

A. Schmittner, College of Oceanic and Atmospheric Sciences, 104 Ocean Admin. Bldg., Oregon State University, Corvallis, Oregon 97331, USA. (aschmittner@coas.oregonstate.edu)